

2-[C-11]Thymidine Imaging of Malignant Brain Tumors¹

Janet F. Eary,² David A. Mankoff, Alexander M. Spence, Mitchel S. Berger, Adam Olshen, Jeanne M. Link, Finbarr O'Sullivan, and Kenneth A. Krohn

Division of Nuclear Medicine [J. F. E., D. A. M., A. O., J. M. L., F. O'S., K. A. K.], and Departments of Neurology [A. M. S.] and Neurosurgery [M. S. B.], University of Washington Medical Center, Seattle, Washington 98195-6113

ABSTRACT

Malignant brain tumors pose diagnostic and therapeutic problems. Despite the advent of new brain imaging modalities, including magnetic resonance imaging (MRI) and [F-18]fluorodeoxyglucose (FDG) positron emission tomography (PET), determination of tumor viability and response to treatment is often difficult. Blood-brain barrier disruption can be caused by tumor or nonspecific reactions to treatment, making MRI interpretation ambiguous. The high metabolic background of the normal brain and its regional variability makes it difficult to identify small or less active tumors by FDG imaging of cellular energetics. We have investigated 2-[C-11]thymidine (dThd) and PET to image the rate of brain tumor cellular proliferation. A series of 13 patients underwent closely spaced dThd PET, FDG PET, and MRI procedures, and the image results were compared by standardized visual analysis. The resulting dThd scans were qualitatively different from the other two scans in approximately 50% of the cases, which suggests that dThd provided information distinct from FDG PET and MRI. In two cases, recurrent tumor was more apparent on the dThd study than on FDG; in two other patients, tumor dThd uptake was less than FDG uptake, and these patients had slower tumor progression than the three patients with both high dThd and FDG uptake. To better characterize tumor proliferation, kinetic modeling was applied to dynamic dThd PET uptake data and metabolite-analyzed blood data in a subset of patients. Kinetic analysis was able to remove the confounding influence of [C-11]CO₂, the principal labeled metabolite of 2-[C-11]dThd, and to estimate the flux of dThd incorporation into DNA. Sequential, same-day [C-11]CO₂ and [C-11]dThd imaging demonstrated the ability of kinetic analysis to model both dThd and CO₂ simultaneously. Images of dThd flux obtained using the model along with the mixture analysis method for pixel-by-pixel parametric imaging significantly enhanced the contrast of tumor compared with normal brain. Comparison of model estimates of dThd transport versus dThd flux was able to discern increased dThd uptake simply on the basis of blood-brain barrier disruption from retention on the basis of increased cellular proliferation. This preliminary study demonstrates the potential for imaging brain tumor cellular proliferation to provide unique information for guiding patient treatment.

INTRODUCTION

Determining brain tumor viability and response to treatment remains problematic because these tumors have highly infiltrative extensions that may or may not disrupt the blood-brain barrier. Most brain tumor imaging methods rely on the visualization of contrast-material leakage over this barrier for diagnosis. With these imaging methods, several important questions for the treatment of patients with malignant brain tumors arise, for instance: (a) what is the grade of the tumor? (b) does it have a heterogeneous growth pattern with regions of higher grade behavior? (c) after surgery, has the tumor been adequately resected and how much viable residual tumor is left? and (d) after radiation treatment, is there remaining tumor in the rim of the

resection cavity that is still viable or proliferating? Alternatively, the therapy may exacerbate the blood-brain barrier disruptions that persist in many patients after treatment; this makes the diagnosis of tumor progression by morphological imaging that depends on the integrity of the blood-brain barrier ambiguous.

The development of adjuvant and novel therapy strategies require monitoring of interim response to treatment increasingly important. These clinical questions can be answered with the use of quantitative imaging that reflects relevant biochemical characteristics of the tumor and its treatment. PET³ using [F-18]FDG has been used to evaluate the grade of primary brain tumor and to distinguish the presence of viable tumor from radionecrosis after treatment (1, 2). FDG reflects tumor energy metabolism and has been a major advance in brain imaging; however, it falls short as an ideal tool for these purposes. The normal brain uptake of FDG obscures subtle increases in uptake by tumor. Also, there are significant tumor-to-tumor differences in the relative metabolism of FDG and glucose. Quantitative tumor growth from a surrogate measure of tumor energetics can be unreliable (3, 4). These difficult imaging issues for the evaluation of brain tumor were the impetus for investigation of the use of 2-[C-11]dThd as an agent for imaging tumor proliferation independent of the blood-brain barrier.

Using labeled dThd for measurement of tumor metabolic rate is not a new concept. Tritiated dThd markers have been widely used in cell culture and animal studies to quantitate tumor DNA synthesis and then to relate these results to effectiveness of cytotoxic tumor agents (5). Our group has been validating the use of [C-11] dThd for a number of years to explore its value in cancer imaging (6-12). dThd is unique among the nucleotides in that it is incorporated only into DNA; there is no dThd in RNA. Our studies using dThd as an imaging agent for determining the regional rate of tumor proliferation (DNA synthesis) showed that these images were often distinctly different from FDG images, with the differences likely relating to tumor energetics metabolism (13). Tumors that responded to chemotherapy had low dThd uptake after treatment, yet often retained modest levels of FDG metabolism. There are mixed reports regarding the utility of FDG uptake and eventual treatment response. In one study, levels of FDG metabolism soon after treatment did not seem to be predictive of eventual treatment response for patients with glioblastoma multiforme (14). However, Alavi *et al.* (15) found that in a majority of cases, post-radiotherapy uptake of FDG was predictive of response.

Studies by Lonneux *et al.* (14) with methyl-[C-11]dThd, showed that the metabolism of this molecule, which results in labeled thymine and several labeled degradation products, yielded uninterpretable images. Because our earlier efforts with this approach to dThd labeling yielded similar results, we have since pioneered development and validation of [C-11]-dThd labeled in the ring-2 position (8, 10, 12, 15, 16), building on the work of Vander Borgh (17). Although this derivative is metabolized *in vivo* at the same rate as the methyl derivatives, the dominant metabolic product carrying the label is [C-11]CO₂ whose pharmacokinetics are well described by existing models for imaging brain tumors (18, 19).

³ The abbreviations used are: PET, positron emission tomography; FDG, fluorodeoxyglucose; dThd, thymidine; MRI, magnetic resonance imaging; ROI, region(s) of interest.

Received 6/12/98; accepted 11/24/98.

The costs of publication of this article were defrayed in part by the payment of page charges. This article must therefore be hereby marked *advertisement* in accordance with 18 U.S.C. Section 1734 solely to indicate this fact.

¹ Supported in part by NIH/National Cancer Institute Grant CA42045.

² To whom requests for reprints should be addressed, at University of Washington Medical Center, Division of Nuclear Medicine, Box 356113, Seattle, WA 98195-6113. Phone: (206) 548-4240.

A PET dThd image is the sum of the dThd metabolic processes for delivery, uptake, and retention in DNA by the tumor and degradative metabolism in the whole patient. In the brain, this metabolism causes a special set of image analysis problems. [C-11]CO₂ rapidly crosses the blood-brain barrier and distributes throughout the brain (12, 17–19). However, blood metabolite analysis and kinetic modeling of dynamic data can separate the contributions of [C-11]dThd and [C-11]CO₂. dThd itself is poorly transported across the blood-brain barrier (20) causing concerns that dThd imaging may not be able to separate permeability in regions of blood-brain barrier disruption from authentic DNA synthesis in proliferating tumor. Therefore, included in this report are the results of key control [C-11] dThd studies in four patients where the blood-brain barrier was known to be intact in one case but disrupted in the other three. We have completed initial validation of our 2-[C-11]dThd methods for practical use in patient imaging studies and present this initial analysis of PET imaging for 13 patients with brain tumors. These data include analysis and characterization of the behavior of the main dThd metabolite, [C-11]CO₂, in the brain and a series of patient imaging studies showing the potential advantages of 2-[C-11]dThd imaging. We also tested the potential of this radiopharmaceutical and associated data analysis for separating blood-brain barrier disruption effects from cellular proliferation.

MATERIALS AND METHODS

Patients. Patients with either primary or recurrent brain tumors were referred from the neurosurgery and neuro-oncology services at the University of Washington Medical Center (UWMC) for imaging with the combination [F-18]FDG and [C-11]dThd. A subset of patients also received [C-11]CO₂ before the dThd study. Before PET imaging, they underwent standard MRI, which included gadolinium-enhanced T1-weighted imaging. Patients provided written informed consent in accord with the Human Subjects and Radiation Safety Committees of the University of Washington. Clinical data for each patient were collected on standardized forms that included initial patient evaluation information (tumor site, size, stage, and histology) as well as subsequent follow-up information, assessment of tumor response, and long-term disease status.

Radiopharmaceuticals. [F-18]FDG was synthesized in the radiochemistry laboratory by minor modifications to the method described by Hamacher (21). [F-18]fluoride from a 30-min irradiation of [O-18]-enriched H₂O generates nominally 150 mCi of FDG. 2-[C-11]dThd synthesis is based on the method of VanderBorgh (17, 22) as modified by our group (16). This automated synthesis involves the sequential conversion of labeled cyanide to cyanate, which is then condensed with ammonia to form urea. The ring closure of [C-11]urea with precursor is done in oleum and then neutralized before the thymine is converted to dThd using an enzyme. The labeled dThd is purified by preparative high performance liquid chromatography producing a yield of 25–40 mCi from a 40-min irradiation. 2-[C-11]dThd for patient research is prepared under permission of an approved protocol of the University of Washington Medical Center Radioactive Drug Research Committee.

[C-11]CO₂ is produced by irradiating nitrogen gas containing 1% O₂ with protons. The ¹⁴N(p,α) reaction for 2-min 40 μA yields approximately 300 mCi. The target contents are then removed by expanding into a stainless steel trap. The trap is maintained at liquid argon temperature to retain all of the CO₂ but not [C-11]CO or [N-13]N₂, which are also produced during irradiation. After the target has emptied, the cold trap is flushed with high purity nitrogen gas and then warmed to release the [C-11]CO₂, which is bubbled into a 10-ml glass serum vial filled with 7 ml of PBS USP (pH 7.2) for the final product formulation of [C-11]CO₂-aqueous. [C-11]CO₂-aqueous is also prepared under permission of a University of Washington Medical Center Radioactive Drug Research Committee-approved protocol.

Patient Imaging. In the imaging protocol, patients were first imaged with the [C-11]-radiopharmaceuticals followed by [F-18]FDG. When a patient arrived in our PET suite, an i.v. line was placed for radiopharmaceutical administration, and an arterial line was placed for blood sampling. The patient was positioned on the imaging table; a foam head restraint and thermoplastic

mask were used for stabilizing this position for acquisition of attenuation images. Ten to 20 mCi 2-[C-11]dThd was infused i.v. for 60 s using a Harvard infusion pump. Imaging was performed on a General Electric Advance Tomograph (GE Medical Systems, Waukesha, WI) starting with infusion of the labeled dThd and continuing for a total of 60 min. Brain images were acquired as dynamic three-dimensional data sets and were reconstructed using standard three-dimensional reprojection reconstruction algorithms onto 35 × 128 × 128 matrices using 4-mm transverse and 8.5-mm axial filters. This resulted in images with 4–6-mm resolution in both the axial and transverse direction (23). The dynamic imaging sequence was as follows: (a) 1 min prescan (injection started); (b) 4 × 20 s; (c) 4 × 40 s; (d) 4 × 60 s; (e) 4 × 3 minutes; and (f) 8 × 5 minutes. Blood sampling and metabolite analyses were performed on all of the patients as described previously (12). Twenty-five arterial blood samples were obtained throughout the imaging study. A 0.2-ml aliquot of each blood sample was pipetted into a test tube with 0.8 ml of 0.5 [smcap]n NaOH to fix CO₂, capped, and counted in the calibrated scintillation well counter. On seven samples another 0.2 ml aliquot was pipetted into a test tube with 0.6 ml of isopropanol, followed by 0.2 ml of 0.5 N HCl. After vortexing, these samples were bubbled with argon to remove the labeled CO₂ to a vent before counting the remainder in the well counter. On three samples, aliquots of blood (0.4 ml) were assayed for labeled dThd *versus* non-CO₂ metabolites by high performance liquid chromatography, using the methods described previously (12). This procedure provided the time course of blood activity for [C-11]dThd, [C-11]CO₂, and C-11-labeled non-CO₂ metabolites that served as inputs in the kinetic analysis of dynamic dThd PET images (8).

Calibration of the counting equipment was performed weekly using vials containing [F-18] that were imaged in the tomograph and then sampled and assayed in the well counter and the dose calibrator. This procedure allowed for blood and image data to be expressed in common units of μCi/ml.

Patient imaging with [C-11]CO₂ took place starting 60 min before the 2-[C-11]dThd study. Up to 10 mCi [C-11]CO₂ in buffered saline was infused i.v. over 2 min, followed by 60 min of dynamic imaging using the same imaging sequence as for dThd studies. Arterial blood samples were collected as described above, with aliquots added to NaOH to retain CO₂.

Imaging with [F-18]FDG took place at the completion of the C-11 imaging studies. Collection of imaging data were initiated; and 60 s later, 10 mCi of FDG was infused i.v. by a Harvard pump (South Natick, MA) i.v. over 2 min. Imaging was continued for 60 min using the same imaging sequence as for the dThd studies, and blood samples were drawn in the same sequence also. The first, middle, and final blood samples were examined for glucose concentration using a Beckman II glucose analyzer (Beckman Instruments, Brea, CA). Serum glucose levels were used in the calculation of the FDG metabolic rate.

All patients underwent MRI for comparison with the PET studies. PET images were compared with gadolinium-enhanced T1-weighted transaxial images. The PET and MRI images could be coregistered by reslicing and reorienting the PET images using anatomical landmarks. This provided an approximate coregistration for qualitative comparison of the studies.

Image Analysis. In the 13 patients studied, the appearance of the MRI, summed FDG, and summed dThd images were compared visually. The level of abnormality in the brain tumor region was rated on a scale of 0, tracer uptake less than or equal to normal brain; 1, mildly abnormal enhancement or tracer uptake; or 2, frankly abnormal enhancement of tracer uptake. Grids of the results comparing dThd uptake *versus* FDG uptake, TdR uptake *versus* MRI, and FDG uptake *versus* MRI were generated. Studies were graded by two experienced observers (J. F. E and D. A. M); differences were resolved by consensus.

To investigate the utility of kinetic analysis of the dynamic dThd images, a subset of studies was also analyzed by a compartmental model of 2-[C-11]dThd and its metabolites (8). This model is depicted in Fig. 1 and accounts for the behavior of dThd, CO₂, and non-CO₂ metabolites (mostly dThd and dihydrothymine) using three compartment sets driven by blood input functions obtained from blood sampling and metabolite analysis. CO₂ kinetics are modeled as described by Buxton (19), including a compartment for tissue CO₂ and bicarbonate, along with a compartment representing CO₂ incorporated into larger molecules. The transport of CO₂ and dThd into brain tissue differ significantly (20), and therefore, blood-tissue transport was estimated independently for each of the compartment sets. This is in contrast to our earlier approach for somatic tumors (8), in which the transport rates of the different labeled species are similar.

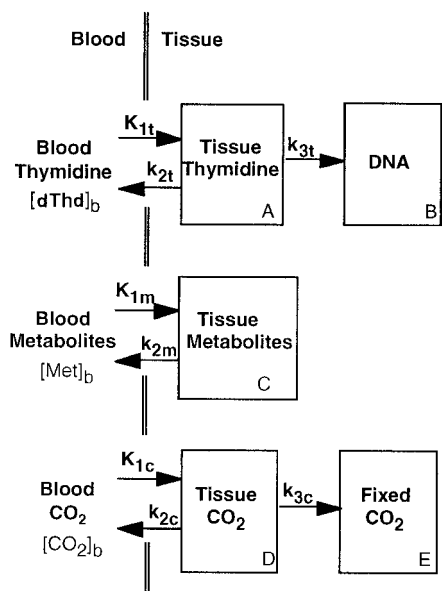


Image Total = A + B + C + D + E + $V_b([dThd]_b + [Met]_b + [CO_2]_b)$

Fig. 1. Compartmental model of 2-[C-11]dThd kinetics. *dThd*, thymidine.

Table 1 Patients studied with *dThd* PET

Tumor types	Patients
Glioblastoma multiforme	4
Anaplastic astrocytoma	7
PNET ^a	1
Adenoid cystic carcinoma	1

^a PNET, peripheral neuro-ectodermal tumor.

For kinetic analysis, time-activity curves were obtained by ROI analysis of the dynamic *dThd* images. MRI and summed *dThd* images were aligned and a set of ROI was drawn to include areas of abnormal contrast enhancement on MRI. In one patient without abnormal contrast-enhancement, regions were drawn corresponding to an area of markedly abnormal signal on T2-weighted MRI images. Whole-brain regions were drawn to include the hemisphere contralateral to the tumor above the level of the caudate nucleus. Tumor and whole-brain regions excluded ventricular and large vascular structures.

Three patients underwent combined CO₂/*dThd* studies. In these studies, kinetic analysis using the compartmental model was applied to the combined dynamic blood and tissue data for both tracers. A single set of parameters was estimated by simultaneously optimizing the fit of the model to both the CO₂ and *dThd* data. One patient with an active gliosarcoma received *dThd* only. For this study the CO₂ parameters were estimated from the whole-brain data (in which *dThd* permeability is limited; Ref. 20) and served as the values for the CO₂ parameters for the estimation of tumor *dThd* parameters. Kinetic parameters were estimated by optimizing model fits of the total tissue time-activity curves obtained from ROI analysis. The flux constant for *dThd* incorporation into DNA (K_{dThd}) was calculated as follows (8):

$$K_{dThd} = \frac{K_{1t}k_{3t}}{k_{2t} + k_{3t}} \quad (1)$$

Pixel-by-pixel images of *dThd* flux were generated by the application of the model in Fig. 1 to the complete three-dimensional dynamic image set using mixture analysis (24). In this approach, dynamic images are segmented by identifying pixels with similar time courses, producing a set of subtime activity curves (typically 20 - 50) that describe the dynamic data set. Through an iterative process, a set of combination constants is then calculated for each image pixel that describes that pixel's time-activity curve as a linear combination or "mixture" of the sub-time-activity curves. The compartmental model is then applied to each sub-time activity curve to estimate *dThd* kinetic

parameters as described above for the ROI data sets. Parameter values for each pixel are then calculated as a linear combination of the parameter values for each sub-time activity curve using the combination constants previously calculated for that pixel. The advantage of this approach is that pixel-by-pixel parametric images can be generated from a reduced set of sub-time-activity curves, reducing statistical variability by combining data from many similar pixels. These sub-time-activity curves are better suited for compartmental analysis than are individual pixel time-activity curves or operator-drawn ROI. Mixture analysis also avoids the computationally intensive task of repeating compartmental analysis for individual image pixels. This approach underwent detailed validation against standard ROI analysis for other compartmental models (25) and preliminary validation for the *dThd* compartmental model.

RESULTS

Thirteen patients received [C-11]*dThd* studies in combination with FDG. Four patients also received a [C-11]CO₂ study before their *dThd* study for the purpose of evaluating the model predictions of CO₂ kinetics. There was a variety of intermediate and high grade brain tumors (Table 1). Three patients had clinically obvious recurrent tumors by MRI and clinical course; 10 had equivocal appearance for the presence of tumor on MRI several months to years after radiation treatment and resection; and one had an intact low-grade tumor that had undergone previous biopsy but had not otherwise been treated.

The results of qualitative image analysis (Table 2) show that approximately one-half of the observations between *dThd* and MRI or FDG showed significant differences on visual inspection of images. There were no consistent patterns that emerged between different types of scans, as evidenced by the similar degree of disparity of *dThd* versus FDG, *dThd* versus MRI, and FDG versus MRI. This was an analysis using a simple grading scale. The next step in image analysis, uptake ratios between tumor and white matter, was not performed because of the complex kinetics of labeled *dThd*. Variability in uptake had sufficiently high variance that tumor and normal brain tissue activity is presented as the quantitative metabolic rate (Table 5).

dThd uptake was more apparent than FDG uptake in four patients (Table 3). One patient had a recurrence after tumor resection, chemotherapy, and radiation therapy with clinical and MRI progression shortly after the time of the PET studies. FDG showed faint uptake compared with normal brain, which was considered mildly abnormal (category 1); treatment necrosis is expected to have no FDG uptake (2). *dThd*, on the other hand, showed markedly abnormal uptake in the tumor site compared with normal brain (Fig. 2A-C). In another patient with an untreated noncontrast-enhancing low-grade glioma, FDG showed no abnormal uptake, whereas *dThd* showed mildly abnormal uptake. One patient with a previously resected intermediate-grade astrocytoma had mildly abnormal *dThd* uptake but no abnormal FDG, and uptake had no residual tumor by subsequent biopsy. A second patient with a previously resected and radiated anaplastic astrocytoma had frankly abnormal *dThd* uptake and mildly abnormal uptake by FDG. That patient was clinically stable for 3 months after the studies

Table 2 Visual interpretation of brain images

Image score	dThd			FDG		
	0 ^a	1	2	0	1	2
FDG						
0	0	2	0			
1	0	4	2			
2	1	1	3			
MRI						
0	0	1	0	1	0	0
1	1	5	3	1	4	4
2	0	1	2	0	2	1

^a 0, no abnormality; 1, mildly abnormal tracer uptake or contrast enhancement; 2, markedly abnormal tracer uptake or contrast enhancement.

Table 3 *Imaging results for all brain tumor patients*

Patient	Clinical status	Imaging results ^a		
		MRI	FDG	dThd
Glioblastoma multiforme				
1	s/p resection, residual tumor	2	1	1
2	s/p resection, ? radionecrosis ^b	1	2	1
3	? tumor vs. radionecrosis ^b	1	2	2
4	Tumor, ? edema ^b	1	1	1
Anaplastic astrocytoma				
1	s/p radiation resection, ? tumor ^b	1	2	2
2	Recurrent tumor	1	1	1
3	Tumor vs. radionecrosis	1	1	2
4	Tumor present	1	1	1
5	Tumor vs. radionecrosis	1	2	0
6	Tumor present, s/p resection	1	0	1
7	Nodular rim tumor	2	1	2
PNET ^c				
1	Progressive tumor	2	2	2
Low-grade astrocytoma				
1	Untreated tumor	0	0	1

^a 0, no abnormality; 1, mildly abnormal tracer uptake or contrast enhancement; 2, markedly abnormal tracer uptake or enhancement.

^b Unclear status.

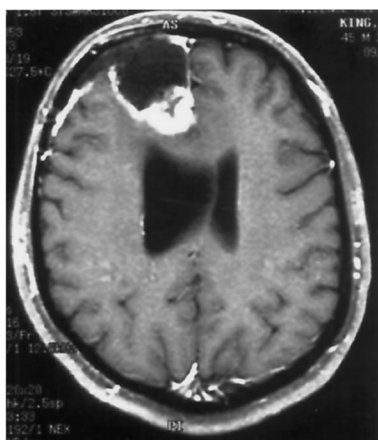
^c PNET, peripheral neuro-ectodermal tumor.

but subsequently had rapid tumor progression. The other two patients, who had dThd uptake, did not appear to have active tumor at the time of the dThd study, and they had mildly abnormal MRI contrast-enhancement.

Two patients had dThd uptake that was less abnormal than FDG uptake. Both had frankly abnormal FDG, one with mildly abnormal dThd uptake and one with no abnormal dThd uptake. Both had high-grade gliomas that had been previously resected and radiated. Both had mildly abnormal MRI contrast-enhancement. One patient is stable without clinical or MRI evidence of progression 10 months after his PET studies. The other patient showed evidence of disease progression but is alive several months after PET imaging.

CO₂ has rapid transport across the blood-brain barrier (18, 19), whereas dThd has more limited transport (20). Examination of the dThd summed image in Fig. 2 shows high background in the normal cortex, most likely on the basis of [C-11]CO₂ that has accumulated from dThd metabolism elsewhere in the body. To investigate the use of kinetic analysis to separate the contribution of CO₂ and quantify dThd retention, a subset of studies (4) was investigated in greater

A.



B.

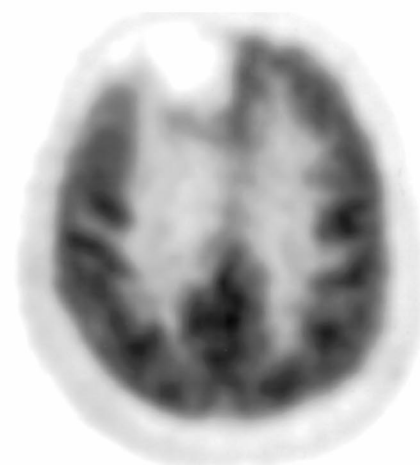
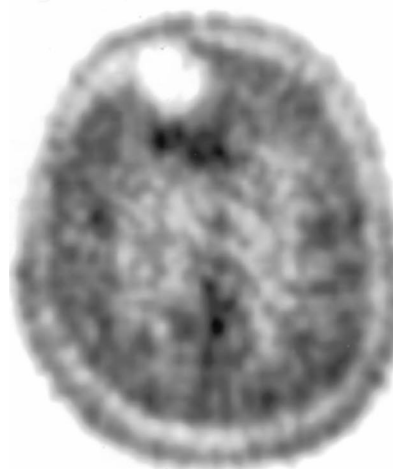
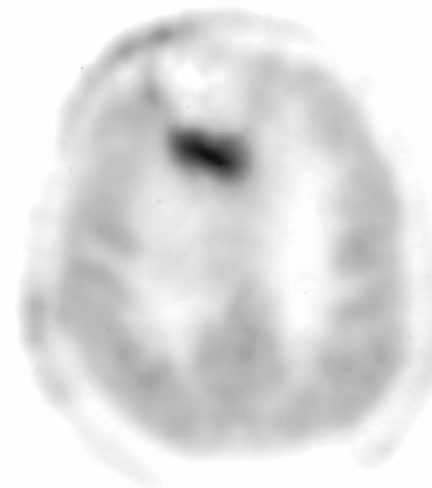


Fig. 2. dThd images of a patient with a recurrent right frontal glioma. A, contrast-enhanced MRI; B, FDG; C, summed 20- 60 min dThd image; D, dThd flux constant image from using the compartmental model and mixture analysis. Note the clear focus of increased dThd flux in the posterior aspect of the tumor dThd resection cavity.

C.



D.



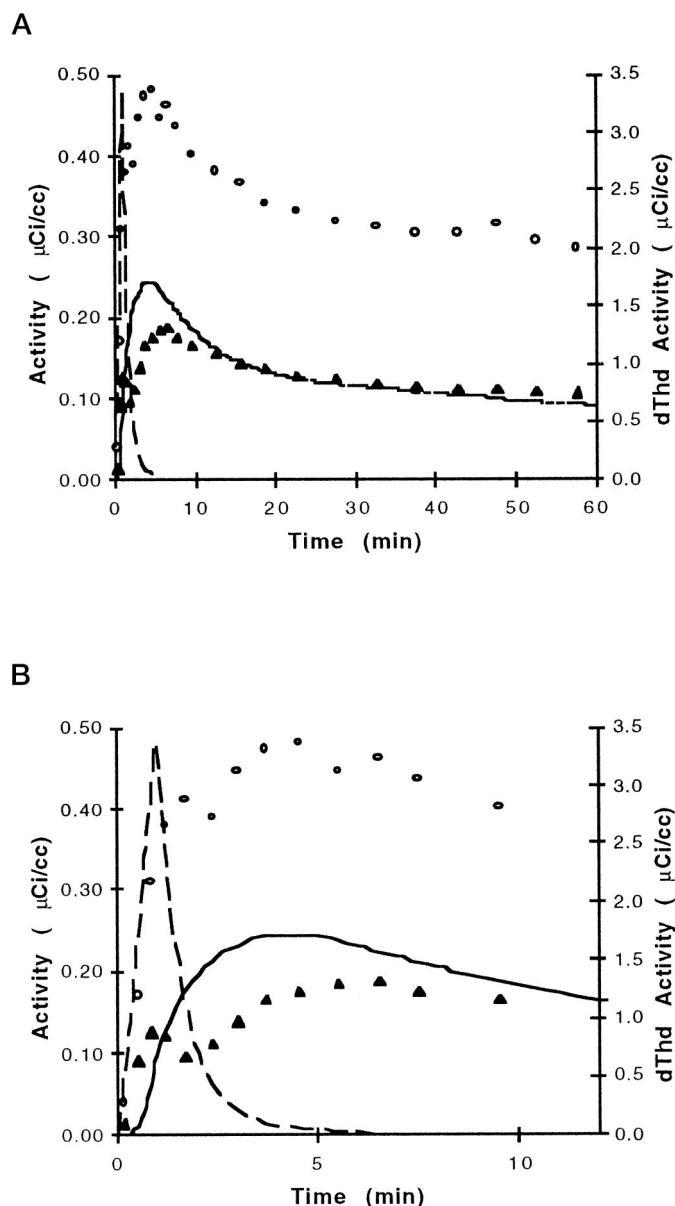


Fig. 3. Time-activity curves for brain tumor patients. A, 0–60 min curves; B, curves with front ends expanded. This patient had an active gliosarcoma (patient 3 of Table 4). CO₂ blood (—); whole blood (▲); tumor (○); dThd blood (---).

detail. Examples of blood and tissue time-activity curves from a patient with an active, high-grade gliosarcoma are shown in Fig. 3. Tissue time-activity curves (Fig. 3) were quantitatively and qualitatively different for tumor *versus* normal brain. The whole brain time-activity curve had a clearly defined early peak the timing of which corresponded to dThd activity in the blood as it passed through brain tissue. This early peak was followed by a broader plateau that corresponded in time to the appearance of the [C-11]CO₂ metabolite in the blood. Tumor, in comparison, had a time-activity curve that peaked and plateaued early, which suggested significant dThd uptake and retention by tumor tissue.

To test the ability of the kinetic model to describe both dThd and CO₂ kinetics, studies using sequential injections of [C-11]CO₂ and 2-[C-11]dThd in patients were performed. The model was simultaneously fit to the time-activity curves after CO₂ and dThd injection. This was performed for both tumor and whole-brain regions. Fig. 4 shows the time-activity curves and model solutions for a representa-

tive study of a patient with a previously treated high-grade glioma. Estimated parameter values for this data set are shown in Table 4. Both the tumor and whole-brain curves in Fig. 4 show good fits of the data using a single set of CO₂ parameters to describe the total curve in the first injection ([C-11]CO₂-aqueous) and the [C-11]CO₂ metabolite fraction after injection of dThd in the second curve. The resulting CO₂ parameters fall within the range of values obtained in previous studies of [C-11]CO₂ in the brain (19). The blood-to-tissue dThd transport constant (K_{1T}) for whole brain is consistent with the studies of dThd transport in the brain by Cornford (20).

The differences between the shapes of the tumor and normal brain curves suggest that kinetic analysis should be able to separate the contribution of dThd uptake and retention from the largely reversible uptake of CO₂. The image in Fig. 2D demonstrates the application of the kinetic model and mixture analysis to the dynamic dThd images and is an image of dThd flux, which indicates the rate of dThd incorporation into DNA with the model correction for labeled metabolites. Comparison of the dThd summed and dThd flux images from mixture analysis (Fig. 2C *versus* 2D) shows the suppression of normal brain background and significant enhancement of tumor contrast in the calculated image, which results in much better definition of the extent of active tumor.

The demonstration of increased dThd uptake in two patients with contrast enhancement on MRI but without active tumor shows that transport across an abnormal blood-brain barrier may contribute to increased dThd uptake, even in the absence of incorporation into DNA. To examine the relative importance of flux *versus* transport, we compared model estimates of transport (K_{1T}) and flux (K_{dThd}) in four patients with increased dThd accumulation at the tumor site (Table 5). These patients had a diverse group of clinical presentations: (a) patient 1 had contrast-enhancing radionecrosis in the left temporal region resulting from neutron therapy of an adjacent sinus tumor (not

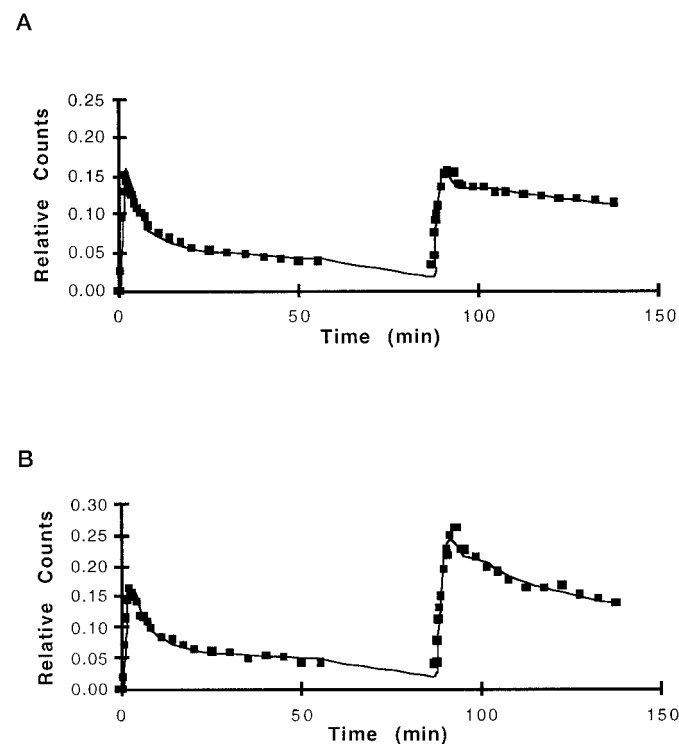


Fig. 4. Model fits of sequential [C-11]CO₂ and [C-11]dThd studies for whole-brain region (A) and tumor region (B). The patient (patient 2 in Table 4) had a previously treated glioblastoma that was contrast-enhancing on MRI but did not have FDG accumulation. Data have been decay-corrected to the time of tracer injection.

Table 4 Model parameter estimates for a sample combined CO₂/dThd study

Parameter	Symbol	Units	NI brain ^a	Tumor
Blood volume	V _b	ml/g	0.041	0.038
dThd blood-tissue transfer constant	K _{1t}	ml/min/g	0.016	0.047
dThd tissue volume	K _{1t} /k _{2t}	ml/g	0.560	1.450
DNA incorporation constant	k _{3t}	1/min	0.015	0.008
dThd flux rate	K _{dThd}	ml/min/g	0.006	0.009
CO ₂ blood-tissue transfer constant	K _{1c}	ml/min/g	0.640	0.530
CO ₂ tissue volume	K _{1c} /k _{2c}	ml/g	0.670	0.790
CO ₂ fixation constant	k _{3c}	1/min	0.005	0.004

^a NI, normal.

included in the previous qualitative analysis of uptake in patients with brain tumors); (b) patient 2 (in Table 3, patient 3, anaplastic astrocytoma) had an area of contrast-enhancement in a previously treated anaplastic astrocytoma with only mildly abnormal FDG accumulation and remained stable clinically for 3 months after imaging); (c) Patient 3 had a high-grade poorly differentiated frontal gliosarcoma (peripheral neuro-ectodermal tumor) that progressed despite brachytherapy subsequent to imaging; and (d) patient 4 had a biopsy-proven, untreated grade II astrocytoma with no contrast-enhancement on MRI. Patients 1, 2, and 4 received sequential CO₂/dThd injections, whereas patient 3 underwent dThd imaging only. In each patient, model estimates of transport and flux obtained from kinetic analysis of ROI data were recorded for both the whole-brain and the lesion site. The lesion:whole-brain ratio was calculated for both transport and flux. The relative increase in flux *versus* transport was calculated as the ratio of lesion:whole-brain ratios for flux *versus* transport, *i.e.*, a ratio of ratios. This measure reflects the relative importance of flux *versus* transport in causing increased uptake. A ratio of less than one indicates increased uptake on the basis of transport but suggests a contribution from tracer retention.

Patients 1 (with radionecrosis) and 2 (with stable anaplastic astrocytoma) had increased dThd accumulation by visual analysis, and flux was elevated in the lesion in comparison with normal brain. However, their low flux relative to transport suggests that transport rather than DNA incorporation was responsible for the increased [C-11]dThd accumulation in the lesion in both cases. In the patient with an active high-grade tumor (patient 3), the relative increase in flux *versus* transport was significantly higher than one, which suggests substantial dThd retention on the basis of incorporation into DNA. In patient 4 (with low-grade tumor and minimal blood-brain barrier breakdown evidenced by the lack of MRI contrast enhancement), dThd flux was only mildly increased in tumor in comparison with normal brain; however, the flux was elevated by 30% more than transport, again suggesting that the increased dThd uptake was on the basis of DNA incorporation.

DISCUSSION

This initial patient series suggests that dThd images can demonstrate the presence of viable tumor in regions where the FDG uptake is too subtle to confidently distinguish tumor from the highly variable levels of FDG uptake of the normal brain. In some cases, the dThd images show clear delineation of tumor from normal brain. This suggests that tumor viability based on an image of cell proliferation may be a more sensitive means for monitoring disease activity than merely looking for the presence or absence of FDG uptake. Delineation of viable tumor is further enhanced by kinetic analysis to separate dThd retention from the background of labeled metabolites. This is illustrated by the clinical situation represented in Fig. 2. This patient had undergone surgery, radiation therapy, and chemotherapy for a right frontal glioblastoma multiforme, and the ambiguous pattern of contrast-enhancement on MRI evolved over the 6–9 months after radiation and chemotherapy. Although FDG imaging showed persistent uptake surrounding the tumor site, the level of uptake was similar to the white matter background uptake. The dThd flux image showed a clear area of increased flux corresponding to a portion of the contrast-enhancing region on MRI. dThd imaging results suggested the location of viable tumor in a pattern distinct from FDG and contrast-enhanced MRI.

This initial series of patients shows that imaging with 2-[C-11]dThd in a clinical setting is feasible. This protocol was well tolerated. The importance of kinetic analysis for discriminating viable tumor from blood-brain barrier disruption has been demonstrated. Equally important is that sufficient 2-[C-11]dThd is taken up in the brain so that low-grade tumors without apparent blood-brain barrier disruption can be identified. [C-11]dThd imaging also shows advantages over FDG imaging. The parametric image of the rate of tumor proliferation based on the rate of uptake of dThd is an additional quantitative measure that has direct clinical use. It can provide a detailed image of the regions of proliferation of the tumor and may be highly sensitive to changes in tumor growth in response to treatment. Ongoing studies are testing this hypothesis. A dThd quantitative image is a valid clinical tool, and model-based analysis used to generate the parametric images accounts for both transport and incorporation of dThd into DNA. This is of particular value in the assessment of early treatment response to determine whether a therapy is effective and whether it should be continued or abandoned in search of a more aggressive therapy.

In the future, because PET dThd imaging yields sensitive quantitative data on the rate of tumor proliferation, it will also be useful in following the course of experimental therapies in which there is risk but also great promise if therapeutic effectiveness could be determined accurately throughout the course of treatment. Because of these

Table 5 dThd parameters in patients imaged with [C-11] dThd and [C-11] CO₂.

Parameter	Patient 1, pure necrosis ^a		Patient 2, treated tumor ^b		Patient 3, active tumor ^c		Patient 4, low-grade tumor ^d	
	Whole-brain	Lesion	Whole-brain	Lesion	Whole-brain	Lesion	Whole-brain	Lesion
V _b (ml/g)	0.053	0.043	0.041	0.038	0.035	0.054	0.038	0.040
K _{1t} (ml/min/g)	0.008	0.059	0.016	0.047	0.006	0.106	0.035	0.030
K _{dThd} (ml/min/g)	0.007	0.021	0.006	0.009	0.0004	0.05	0.011	0.012
Lesion:Whole-brain ratios								
K _{1t}	7.4		2.9		17.7		0.9	
K _{dThd}	3.0		1.5		125.0		1.1	
Relative increase in flux <i>versus</i> transport ^e	0.4		0.5		7.1		1.3	

^a Neutron therapy of sinus tumor; pure radiation necrosis.

^b Contrast enhancing lesion on MRI after therapy of glioblastoma; clinically stable at 3-mon follow-up.

^c Active gliosarcoma.

^d Untreated grade II astrocytoma.

^e Relative increase in flux *versus* transport = lesion:whole-brain ratio for flux (K_{dThd}) divided by lesion:whole-brain ratio for transport (K_{1t}), *i.e.*, ratio of ratios.

characteristics, dThd imaging may play a role in the assessment of tumor grade, providing information on tumor growth rate and metastatic potential. This preliminary patient series demonstrates that PET imaging with [C-11]dThd for quantifying tumor proliferation in the brain noninvasively is sensitive and feasible, setting the stage for its use in more compelling clinical oncology applications.

ACKNOWLEDGMENTS

We thank Barbara Lewellen, Thomas Lewellen, and Steve Kohlmyer for imaging support and Holly Pike and Gregory Cotter for editorial assistance.

REFERENCES

- Di Chiro, G., and Brooks, R. PET-FDG of untreated and treated cerebral gliomas. *J. Nucl. Med.*, 29: 421–422, 1988.
- Di Chiro, G., Oldfield, E., Wright, D. C., De Michele, D., Katz, D. A., Patronas, N. J., Doppman, J. L., Larson, S. M., Ito, M., and Kufta, C. V. Cerebral necrosis after radiotherapy and/or intra-arterial chemotherapy for brain tumors: PET and neuropathologic studies. *Am. J. Roentgenol.*, 150: 180–197, 1988.
- Kapoor, R., Spence, A. M., Muzi, M., Graham, M. M., Abbott, G. L., and Krohn, K. A. Determination of the deoxyglucose and glucose phosphorylation ratio and the lumped constant in rat brain and a transplantable rat glioma. *J. Neurochem.*, 53: 37–44, 1989.
- Spence, A. M., Muzi, M., Graham, M. M., Freeman, S. D., Berger, M. S., and Ojemann, G. A. Analysis of the deoxyglucose lumped constant in human malignant gliomas. *Ann. Neurol.*, 30: 271–272, 1991.
- Livingston, R., and Hart, J. The clinical applications of cell kinetics in cancer therapy. *Ann. Rev. Pharmacol. Toxicol.*, 17: 529–543, 1977.
- Larson, S. M., Weiden, P. L., Grunbaum, Z., Rasey, J. S., Kaplan, H. G., Graham, M. M., Harp, G. D., Sale, G. E., and Williams, D. L. Positron imaging feasibility studies I: characteristics of [H-3]thymidine uptake in rodent and canine neoplasms: concise communication. *J. Nucl. Med.*, 22: 869–874, 1981.
- Mankoff, D., Shields, A., Graham, M., Link, J., Eary, J., and Krohn, K. A graphical analysis method to estimate blood-to-tissue transfer constants for systems with labeled metabolites. *J. Nucl. Med.*, 37: 2049–2057, 1996.
- Mankoff, D. A., Shields, A. F., Graham, M. M., Link, J. M., Eary, J. F., and Krohn, K. A. Kinetic analysis of 2-[C-11]thymidine PET imaging studies: compartmental model and mathematical analysis. *J. Nucl. Med.*, 39: 1403–1455, 1998.
- Shields, A., Larson, S., Grunbaum, Z., and Graham, M., Short-term uptake in normal and neoplastic tissues: studies for PET. *J. Nucl. Med.*, 25: 759–764, 1984.
- Shields, A., Lim, K., Grierson, J., Link, J., and Krohn, K. Utilization of labeled thymidine in DNA synthesis: studies for PET. *J. Nucl. Med.*, 31: 337–342, 1990.
- Shields, A. F., Graham, M. M., Kozawa, S. M., Kozell, L. B., Link, J. M., Swenson, E. R., Spence, A. M., Bassingthwaite, J. B., and Krohn, K. A. Contribution of labeled carbon dioxide to PET imaging of carbon-11-labeled compounds. *J. Nucl. Med.*, 33: 581–584, 1992.
- Shields, A., Mankoff, D., Graham, M., Zheng, M., Kozawa, S. M., Link, J. M., and Krohn, K. A. Analysis of 2-[carbon-11]thymidine blood metabolites in PET imaging. *J. Nucl. Med.*, 37: 290–296, 1996.
- Shields, A. F., Mankoff, D. A., Link, J. M., Graham, M. M., Eary, J. F., Kozawa, S. M., Zheng, M., Lewellen, B., Lewellen, T. K., Grierson, J. R., and Krohn, K. A. Use of [¹¹C]thymidine and FDG with positron emission tomography (PET) to measure response to therapy. *J. Nucl. Med.*, in press.
- Lonneux, M., Labar, D., Bol, A., Jamar, F., and Pauwels, S. Uptake of 2–11-C thymidine in colonic and bronchial tumors. *In: Metabolic Imaging of Cancer: Proceedings of the European Conference on Research and Application of Positron Emission Tomography in Oncology.* Groningen, the Netherlands: PET-Centrum AZG, 1996.
- Alavi, J. B., Alavi, A., Chawluk, J., Kushner, M., Powe, J., Hickey, W., and Reivich, M. Positron emission tomography in patients with glioma: a predictor of prognosis. *Cancer (Phila.)*, 62: 1074–1078, 1988.
- Link, J. M., Grierson, J., and Krohn, K. Alternatives in the synthesis of 2-[C-11]thymidine. *J. Labelled Compd Radiopharm.*, 37: 610–612, 1995.
- Vander Borgh, T., Labar, D., Pauwels, S., and Lambotte, L. Production of 2-[¹¹C]thymidine for quantification of cellular proliferation with PET. *Appl. Radiat. Isotopes*, 42: 103–104, 1991.
- Brooks, D. J., Lammertsma, A. A., Beaney, R. P., Leenders, K. L., Buckingham, P. D., Marshall, J., and Jones, T. Measurement of regional cerebral pH in human subjects using continuous inhalation of [C-11]CO₂ and Positron Emission Tomography. *J. Cereb. Blood Flow Metab.*, 4: 458–465, 1984.
- Buxton, R., Wechsler, L., Alpert, N., Ackerman, R., Elmaleh, D., and Correia, J. Measurement of brain pH using [C-11]CO₂ and positron emission tomography. *J. Cereb. Blood Flow Metab.*, 4: 8–16, 1984.
- Cornford, E., and Oldendorf, W. Independent blood-brain barrier transport systems for nucleic acid precursors. *Biochim. Biophys. Acta*, 394: 211–219, 1975.
- Hamacher, K., Coenen, H., and Stocklin, G. Efficient stereospecific synthesis of no-carrier-added 2-[¹⁸F]fluoro-2-D-glucose using aminopolyether supported nucleophilic substitution. *J. Nucl. Med.*, 27: 235–238, 1986.
- Vander Borgh, T., Pauwels, S., Lambotte, L., and Beckers, C. Rapid synthesis of 2C-radiolabelled thymidine (2C-dThd), a potential tracer for measurement of liver regeneration. *J. Nucl. Med.*, 30: 929P, 1989.
- Lewellen, T. K., Kohlmyer, S., Miyaoka, R., Schubert, S., and Stearns, C. Investigation of the count rate performance of the General Electric ADVANCE positron emission tomograph. *IEEE (Inst. Electr. Electron. Eng.) Trans. Nucl. Sci.*, 42: 1051–1057, 1995.
- O'Sullivan, F. Metabolic images from dynamic positron emission tomography studies. *Stat. Methods Med. Res.*, 3: 87–101, 1994.
- O'Sullivan, F., Muzi, M., and Graham, M. Parametric imaging by mixture analysis in 3D: validation for dual tracer glucose studies. *Neuro. Imag.*, 2: 556, 1995.

Cancer Research

The Journal of Cancer Research (1916–1930) | The American Journal of Cancer (1931–1940)

2-[C-11]Thymidine Imaging of Malignant Brain Tumors

Janet F. Eary, David A. Mankoff, Alexander M. Spence, et al.

Cancer Res 1999;59:615-621.

Updated version Access the most recent version of this article at:
<http://cancerres.aacrjournals.org/content/59/3/615>

Cited articles This article cites 20 articles, 8 of which you can access for free at:
<http://cancerres.aacrjournals.org/content/59/3/615.full#ref-list-1>

Citing articles This article has been cited by 20 HighWire-hosted articles. Access the articles at:
<http://cancerres.aacrjournals.org/content/59/3/615.full#related-urls>

E-mail alerts [Sign up to receive free email-alerts](#) related to this article or journal.

Reprints and Subscriptions To order reprints of this article or to subscribe to the journal, contact the AACR Publications Department at pubs@aacr.org.

Permissions To request permission to re-use all or part of this article, use this link
<http://cancerres.aacrjournals.org/content/59/3/615>.
Click on "Request Permissions" which will take you to the Copyright Clearance Center's (CCC) Rightslink site.